Since January 2020 Elsevier has created a COVID-19 resource centre with free information in English and Mandarin on the novel coronavirus COVID-19. The COVID-19 resource centre is hosted on Elsevier Connect, the company's public news and information website.

Science of the Total Environment 637–638 (2018) 104–111

Contents lists available at ScienceDirect

Science of the Total Environment

journal homepage: www.elsevier.com/locate/scitotenv

Heteroaggregation of an enveloped bacteriophage with colloidal sediments and effect on virus viability

Al Katz [a], Stephanie Peña [b], Alexandra Alimova [c], Paul Gottlieb [c], Min Xu [d], Karin A. Block [b,*]

[a] Department of Physics Department of Earth and Atmospheric Science, The City College of New York, 160 Convent Ave., New York, NY 10031, United States
[b] Department of Earth and Atmospheric Science, The City College of New York, 160 Convent Ave., New York, NY 10031, United States
[c] Sophie Davis School of Biomedical Education, The City College of New York, 160 Convent Ave., New York, NY 10031, United States
[d] Department of Physics, Fairfield University, Fairfield, CT 06824, United States

HIGHLIGHTS

- Sediments interact with enveloped viruses but effects on viability are unknown.
- Light scattering measured aggregation rates of virus with four mineral types.
- Heteroaggregation was hydrophobic and faster with negatively-charged sediments.
- The greatest reduction in infectivity occurred in virus-montmorillonite aggregates.
- Aggregation with sediment caused virus disassembly and infectivity loss.

GRAPHICAL ABSTRACT

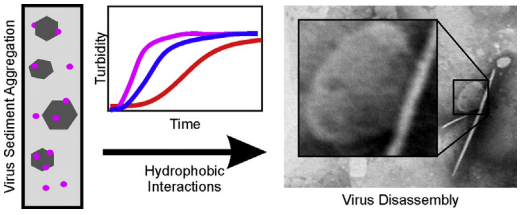

ARTICLE INFO

Article history:
Received 16 March 2018
Received in revised form 27 April 2018
Accepted 30 April 2018
Available online 7 May 2018

Editor: Jay Gan

Keywords:
Virus
Bacteriophage
Clay minerals
Montmorillonite
Aggregation

ABSTRACT

Four sediments in the colloidal size range: goethite, montmorillonite, illite, and kaolinite, were suspended with the bacteriophage φ6, a model enveloped virus, to determine relative rates of heteroaggregation and the effect of aggregation on virus viability. Turbidity was measured on combinations of virus and each sediment type at low concentration to determine aggregation rates. Aggregation of sediment with virus occurred regardless of mineral type, and larger fraction of virus is expected to aggregate with increasing sediment concentration leading to higher deposition rates. The negatively charged sediments, aggregated with φ6 (also negatively charged at neutral pH) at a faster rate than the positively charged sediments, yielding turbidity slopes of 4.94×10^{-3} s^{-1} and 7.50×10^{-4} s^{-1} for φ6-montmorillonite and φ6-illite aggregates, respectively, and 2.98×10^{-5} s^{-1} and 2.84×10^{-5} s^{-1}, for φ6-goethite and φ6-kaolinite, respectively. This indicates that the interaction between sediments and virus is hydrophobic, rather than electrostatic. Large numbers of virions remained viable post-aggregation, despite the fragility of the viral envelope, indicating that small-sized aggregates, which may travel more readily through porous media, may pose an infection risk. The fraction of φ6 that remained viable varied with sediment type, with montmorillonite-φ6 aggregates experiencing the greatest reduction in infectivity at 35%. TEM analyses reveal that in all sediment-φ6 combinations, infectivity loss was likely due to disassembly of the viral envelope as a result of aggregation.

1. Introduction

The mechanisms that influence the transport of viruses are important for management of natural systems and freshwater resources.

* Corresponding author.
E-mail address: kblock@ccny.cuny.edu (K.A. Block).

https://doi.org/10.1016/j.scitotenv.2018.04.425
0048-9697/

These may include human pathogens such as those introduced by fecal matter, but, more importantly, bacteriophage which serve to regulate bacterial populations (O'Brien et al., 2017). Bacteriophage alter biogeochemical cycles through lysis of bacterial cells (Díaz-Muñoz and Koskella, 2014; Koskella and Brockhurst, 2014) and impact eukaryotes that depend on bacterial populations, thus having a significant impact on the greater ecosystem. The distribution and residence time of viruses is affected by the chemistry of the water, e.g., dissolved organic matter, metals, and contaminants, but also the suspended materials, such as particulate organic matter (POM) and suspended sediment, primarily clays, which serve as substrate and habitat for biofilm-producing bacteria (Alimova et al., 2006; Alimova et al., 2009). In fact, sediment-bearing biofilms have been shown to sequester virus particles in wetlands where they are subsequently concentrated and subject to re-release (Flood and Ashbolt, 2000). Furthermore, bacteriophages are utilized as subsurface tracers and indicators for a variety of environmental applications (Ghanem et al., 2018; Keswick et al., 1982; Redman et al., 1997) and, therefore, their interaction with sediments may affect their quantification in hydrological experiments.

An estimated 10^{31} virus particles world-wide are prevalent in both soils and aquatic systems (Breitbart and Rohwer, 2005; Weinbauer and Rassoulzadegan, 2004). In aquatic systems, the length of time in which a virus can interact with potential hosts is largely controlled by sinking rates (Fuhrman, 1999). These rates are strongly influenced by aggregation with suspended particles. Sediments are known to influence virus transport and survival in porous media by controlling the potential for viruses to contaminate groundwater (Jin and Flury, 2002; Chu et al., 2000) and to promote lysis of bacteria in soils (Kimura et al., 2008). The mineralogy and size of suspended sediments affects the extent to which viruses will aggregate and sorb to sediments (Chu et al., 2000; Jin and Flury, 2002; McGechan and Lewis, 2002; Syngouna and Chrysikopoulos, 2015). With a few recent exceptions, enveloped viruses (Block et al., 2016; Block et al., 2014), have been largely omitted from studies of virus-sediment interaction, aggregation, and viability. Enveloped viruses possess different structural properties from non-enveloped viruses and include important plant and animal pathogens such as herpesvirus, coronavirus and Influenza A and B, all of which are found in natural and wastewaters (Batik et al., 1980; Gundy et al., 2008; Rosenberg et al., 1980; Sharp et al., 1975; Stallknecht et al., 1990a; Stallknecht et al., 1990b).

Virus particles typically range from 20 nm to 500 nm in diameter, and are therefore considered colloidal particles. For non-enveloped viruses, the surface charge is determined by the protonation/deprotonation of amino acids in the capsid (Elimelech et al., 1995). However, for enveloped virions, surface charge is determined by envelope proteins and lipids. The colloidal interaction between virus particles and the small fraction of suspended sediments can be described by DLVO theory (Derjaguin and Landau, 1941; Verwey and Overbeek, 1948), in which the potential between colloidal particles is the sum of the attractive van der Waals potential and the Coulomb potential (repulsive for like-charged particles and attractive for oppositely-charged particles). DLVO theory has been extended to include hydrophobic forces (van Oss, 1993; van Oss et al., 1990).

Previous research has shown that for non-enveloped viruses, sorption is largely influenced by hydrophobicity. Chattopadhyay and Puls (1999), (2000) studied the attachment of three, non-enveloped, bacteriophages, T2, MS2 and φX174 to several clay fractions and calculated the electrostatic and hydrophobic contributions to the free energy. Their calculations showed that surface hydrophobicity dictates sorption of viruses to clays. Chrysikopoulos and Syngouna (2012) looked at attachment of the bacteriophages MS2 and φX174 to kaolinite or montmorillonite, and using extended DLVO energy calculations, concluded that the virus-clay attachment was primarily through hydrophobic interaction.

A study of heteroaggregation of the non-enveloped cowpea mosaic virus with colloidal hematite revealed that at pH 6, at which hematite carries a positive surface charge and the virus a negative charge, the aggregates accumulated four times as many viruses as hematite particles Vilker et al. (1994). However, at pH 3, in which both particle types are positively charged, the aggregates contained three times as many hematite particles as virus. From these results, they concluded that attraction between the virus and hematite is mostly governed by electrostatic interactions.

The above studies all investigated non-enveloped viruses which are structurally different to viruses with lipid envelopes (e.g. influenza, paramyxovirus). In this work, we employ turbidity measurements to investigate the heteroaggregation of a model envelope virus, the bacteriophage φ6, with colloidal goethite and three clay minerals: illite, kaolinite and montmorillonite. φ6 is a member of the cystoviridae family of bacteriophage. The cystoviridae are the only phage family with an outer bi-lipid envelope. φ6 is a dsRNA virus whose host cell is *Pseudomonas phaseolicola*, a common plant pathogen. φ6 consists of an icosahedral nucleocapsid surrounded by a bi-lipid envelope and is therefore employed as a model for virus emergence in evolutionary studies and for human pathogens such as coronavirus (Dennehy, 2017; Mindich, 2004). The diameter of φ6 is ~80 nm. The φ6 virus carries negative charge at neutral pH (Block et al., 2014).

Montmorillonite and illite platelets both have positive charged edges and negative charged faces with an overall negative charge at neutral pH (González Sánchez et al., 2008; Van Olphen, 1962). Kaolinite platelets have negatively charged faces, and at neutral pH, negatively charged edges (Gupta et al., 2011; Schroth and Sposito, 1997). Goethite is positively charged at neutral pH (Gaboriaud and Ehrhardt, 2003; Zeltner and Anderson, 1988).

The effect of the interaction of colloidal sediments and enveloped viruses on virus viability, the nature of that interaction is unknown. We will present aggregation rates as determined by turbidity experiments, the effect of the interaction between φ6 and sediments on φ6 infectivity, and discuss the environmental implications of our findings.

2. Turbidity and colloidal aggregation

2.1. Early stage turbidity and colloidal aggregation

In the early stage of colloidal aggregation, suspensions consist mostly of primary particles and aggregation is a bimolecular process in which the kinetics are dominated by the merging of individual primary particles to form doublets: $N + N \rightarrow N_2$ (García-García et al., 2006; García-García et al., 2007). The rate equation for the loss of primary particles into doublets can be written as:

$$\frac{dN(t)}{dt} = -KN^2(t) \tag{1}$$

where $N(t)$ is the number density of particles and K is the aggregation rate constant for doublet formation. The corresponding rate equation for doublet, N_2, formation is:

$$\frac{dN_2(t)}{dt} = \frac{K}{2}N^2(t) \tag{2}$$

Integration of Eq. (1) gives:

$$\frac{1}{N(t)} = \frac{1}{N_0} + Kt \tag{3}$$

where N_0 is the number density of primary particles at $t = 0$. The average number of primary particles in an aggregate is $\eta = N_0/N(t)$ and thus in the early stage of aggregation:

$$\eta(t) = 1 + KN_0t. \tag{4}$$

From Eq. (4) it is seen that in the early growth region, aggregate growth is linear in time (Kobayashi and Ishibashi, 2011; Puertas and Nieves, 1997).

The turbidity (τ) for a system of monomeric colloidal aggregates is given by (Katz et al., 2013):

$$\tau = \eta N L c_0 k^4 a^6 \frac{2\eta}{(D_f-1)(D_f-2)} \frac{1}{(kr)^2}\left[1-\left(1+(kr)^2\right)^{1-D_f/2}\cos\left((D_f-2)\arctan(kr)\right)\right] \quad (5)$$

where L is the optical path length; $k = 2\pi/\lambda$, is the optical wavenumber; $c_0k^4a^6$ is the scattering cross-section of a primary particle; a is the effective primary particle radius; D_f is the fractal dimension of the aggregate; and r is the radius of gyration of the aggregate; ηN is the number density of primary particles and is constant for each individual suspension. In the initial stage of aggregation, the aggregates are small and if the primarily particles are much smaller than the optical wavelength, $kr << 1$. Expanding Eq. (5), and keeping only the lowest order terms in kr, it is seen that $\tau \propto \eta$, i.e. aggregate size, and at early time, $\tau \propto KN_0t$.

2.2. Early stage heteroaggregation

Liu et al. (2007) considered measurements of heteroaggregation rate constants by turbidity for dispersions containing colloids of different sizes. They developed a method based on the T-matrix to evaluate changes in turbidity as two primary particles form a doublet during heteroaggregation. They also considered the effects of multiple scattering on turbidity and determined that multiple scattering effects are not significant when the relative volume of the scatterers is <0.1%.

In the case of heteroaggregation of two distinct primary particles, e.g. viruses and sediments, three types of bi-molecular particle mergers are possible: sediment – sediment; virus – virus; and sediment – virus. Eq. (2) is modified to include the three possible modes of doublet formation (Yu and Borkovec, 2002):

$$\begin{aligned}\frac{dN_{ss}}{dt} &= \frac{1}{2}K_{ss}N_s^2\\ \frac{dN_{vv}}{dt} &= \frac{1}{2}K_{vv}N_v^2\\ \frac{dN_{sv}}{dt} &= K_{sv}N_sN_v\end{aligned} \quad (6)$$

in which N_s and N_v are the number of primary sediment and virus particles in the suspension, respectively; N_{ss}, N_{vv} and N_{sv} are the number of sediment-sediment, virus-virus and sediment-virus doublets, respectively; and K_{ss}, K_{vv} and K_{sv} are the rate constants for sediment – sediment, virus – virus, and sediment – virus doublet formation, respectively.

The light extinction for a system of heteroaggregation is given by a modification of Eq. (5):

$$\tau = \eta N L c_0 k^4 a_{eff}^6 \frac{2\eta}{(D_f-1)(D_f-2)} \frac{1}{(kr)^2}\left[1-\left(1+(kr)^2\right)^{1-D_f/2}\cos\left((D_f-2)\arctan(kr)\right)\right] \quad (7)$$

where a_{eff} is an effective primary particle radius, and the scattering cross-section, c_0, is an average cross-section weighted by the concentrations of each type of primary particle in the aggregate. As in the case of mono-colloidal systems at early times, i.e. early stage of aggregation, $kr << 1$ and, keeping only terms in kr, τ is proportional to η.

3. Materials and methods

3.1. Cystovirus φ6 preparation

Purified cystovirus φ6 was prepared following the procedure described in Katz et al. (2012). After purification, the virus was resuspended in buffer A, modified to have a reduced divalent cation concentration (10 mM KH_2PO_4 and 0.5 mM $MgSO_4$). It was confirmed by counting plaque forming units (PFU) of *P. phaseolicola* infection that φ6 survives in the modified buffer for several days at room temperature.

3.2. Clay preparation

The four mineral types chosen for this study were goethite, kaolinite (City College of New York Rock and Mineral Collection); illite, and montmorillonite (Wards Science, Rochester, NY). Composition and purity of mineral specimens was confirmed by X-ray powder diffraction (City College of New York). All sediments were first crushed into powders and each washed with a 5% sodium hypochlorite (bleach) solution overnight to remove any possible organic matter or microbial contaminants. Sediments were then washed multiple times in distilled water to remove the sodium hypochlorite residue. The small clay fraction (<0.2 μm) was separated by centrifugation in a Sorvall ultracentrifuge (ThermoFisher Scientific, Waltham, MA) with an SS34 rotor at 5000 rpm (3000 g) for 1440 s (montmorillonite), 1140 s (illite), 1200 s (kaolinite) or 720 s (goethite). The supernatants containing the small fraction were collected and sterilized by autoclaving at 121 °C and 100 kPa above atmospheric pressure for 1800 s to eliminate possible bacterial contamination.

3.3. Heteroaggregate formation & turbidity measurements

3.3.1. Turbidity apparatus

Turbidity measurements were performed at 20 °C and pH = 7 with the aggregates in a 1 cm optical path length quartz cuvette. Specimens were illuminated with a broadband halogen lamp (HL2000, Ocean Optics, Inc., Dunedin, FL.) coupled to an optical fiber. Spectra were collected in the wavelength range of 400 nm to 1000 nm. The transmitted light was collected by a second optical fiber coupled to a spectrophotometer equipped with a CCD (HR2000, Ocean Optics, Inc.) which transferred the data to a personal computer. A 1 mm diameter aperture positioned in front of the collection fiber limited data collection to transmitted light while blocking scattered light. A magnetic stirrer was employed to prevent settling of the suspended colloidal aggregates. The distance between the cuvette and aperture was 5 cm, limiting the collection solid angle to 0.00003 sr and thus restricting the intensity of forward scattered light incident on the collection fiber (Katz et al., 2013). For time-resolved measurements, each spectrum was integrated for 250 ms using a high-speed data acquisition mode which allowed rapid collection and transfer of many spectra (3600 spectra for the typical 900 s experiment) to a PC with no dead-time between spectra acquisitions. For the estimation of φ6 concentration by turbidity, spectra were integrated for 30 s.

3.3.2. φ6 Turbidity.

The φ6 concentration was estimated from turbidity, approximating the φ6 virions as spheres with a refractive index of 1.45 and a diameter of 80 nm. The φ6 turbidity is given by (Chýlek and Li, 1995; Xu, 2003; Xu et al., 2003):

$$\tau_v(\lambda) = C_sN_vL \approx \frac{8n_w^2\pi^3r^4}{\lambda^2}\left(\frac{n_v}{n_w}-1\right)^2 N_vL \quad (8)$$

where C_s is the scattering cross section; N_v is the φ6 concentration; L is the optical path length; n_w is the refractive index of water; n_v is the

refractive index of φ6; r is the radius of φ6; and λ is the optical wavelength. φ6 is sufficiently small compared to the wavelength of visible light so that higher order terms can be ignored. Based on the measured turbidity, the stock φ6 concentration was determined to be 7.8×10^{11} cm^{-3}, prior to the 2× dilution incurred when mixed with an equal volume of suspended sediments. This estimate is slightly larger than the estimate from counting PFUs (6.8×10^{11} cm^{-3}) but is likely more accurate as it also includes virions rendered non-infectious due to envelope defects. φ6, due to its lower refractive index and smaller size, scatters less efficiently than the selected sediments. Therefore, for the heteroaggregation turbidity experiments, the φ6 concentration was adjusted to have a lower turbidity than the turbidity at the lowest sediment concentration. The φ6 stock suspension was diluted to have a turbidity of 0.128 at 750 nm.

3.3.3. Heteroaggregation turbidity

Heteroaggregation experiments were performed by mixing 1 ml of suspended φ6 with 1 ml of each suspended sediment. This resulted in a further 50% dilution of the cation concentration (5 mM KH_2PO_4 and 0.25 mM $MgSO_4$). Due to both the larger volume of the sediment primary particles (~0.2 μm) and higher refractive index. Refractive indices of the three sediment types are (geometric mean of the three axes): goethite: $n = 2.18$; illite: $n = 1.58$; kaolinite: $n = 1.56$; montmorillonite: $n = 1.55$ (Deer et al., 1992; Shannon et al., 2002; Weidler and Friedrich, 2007) compared to φ6 particles (80 nm), the sediment primary particles have a higher scattering cross-section than the virions. Therefore, the heteroaggregation experiments were performed using a higher concentration of viral particles than sediments. The sediment concentrations were adjusted to have a turbidity of ~0.6 (after 2× dilution by addition of virus suspension) at 750 nm – a wavelength in which light extinction losses are primarily due to scattering rather than absorption. The concentrations were chosen so that the total volume of the scatterers was <0.1% of suspension volume, thus staying in the single scattering regime and keeping the incidence of multiple scattering small (Katz et al., 2013; Wind and Szymanski, 2002; Xu and Sun, 2010), while still providing a reasonable signal-to-noise level. The sediment and virus concentrations after the 2× dilution are summarized in Table 1.

After completion of the turbidity measurements, the suspensions were centrifuged at 13,000 rpm (16,000 g) for 600 s. The centrifugation was sufficient to pellet the smallest heteroaggregates (i.e. doublets) and individual sediment primary particles but not individual virions. The pellets were resuspended in buffer and both the resuspended pellets and supernatants were analyzed for the presence of φ6 proteins by SDS-PAGE.

3.4. SDS-PAGE

The separated heteroaggregate pellets and supernatants were analyzed by SDS-PAGE (Studier, 1973). The fraction of φ6 in the pellets was estimated by analyzing the relative densities of the P1, P2 and P3 protein bands of the heteroaggregate pellets and supernatants. It is noted that the SDS-PAGE experiment does not resolve P1 and P2 due to the closeness of their molecular weight (85 kDa and 75 kDa,

Table 1
Concentrations of colloidal particles.

	Concentration mg cm^{-3}	Primary particles cm^{-3}
Goethite	0.096	5.3×10^9
Illite	1.9	9.6×10^{10}
Kaolinite	0.66	3.9×10^{10}
Montmorillonite	1.6	9.6×10^{10}
φ6		3.9×10^{11}

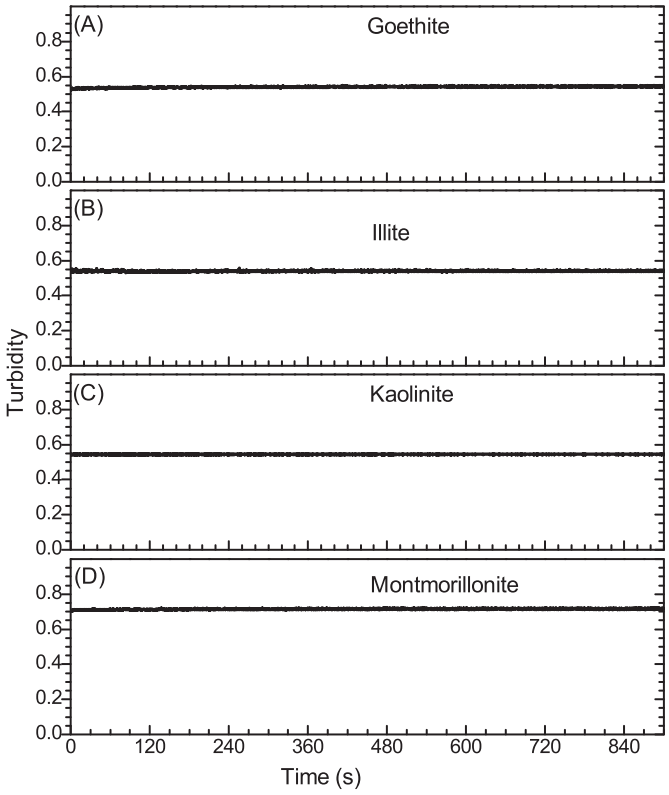

Fig. 1. Turbidity (λ = 750 nm) of sediments in reduced cation buffer for (A) Goethite; (B) Illite; (C) Kaolinite; and (D) Montmorillonite.

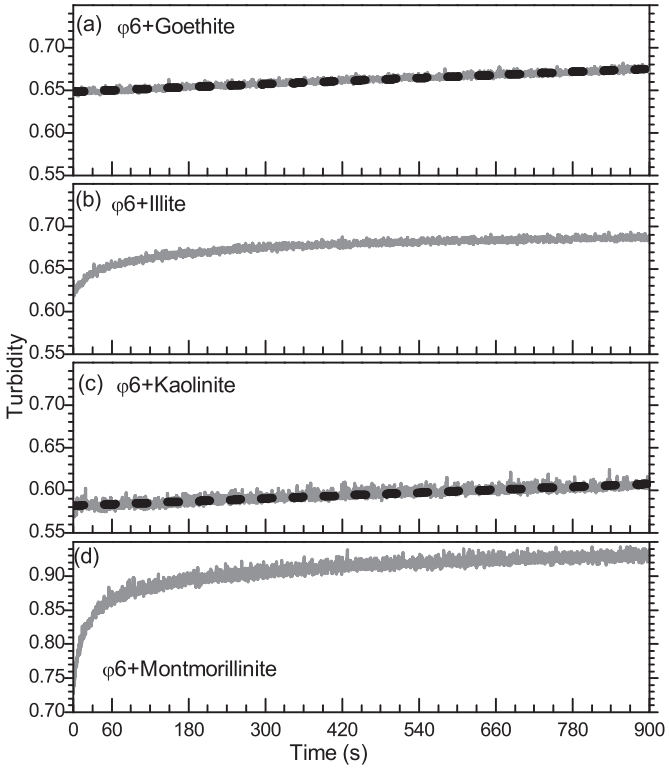

Fig. 2. Time evolution of turbidity (λ = 750 nm) for heteroaggregation of φ6 with (A) Goethite; (B) Illite; (C) Kaolinite; and (D) Montmorillonite. Linear fits for goethite and kaolinite are shown as gray diamonds.

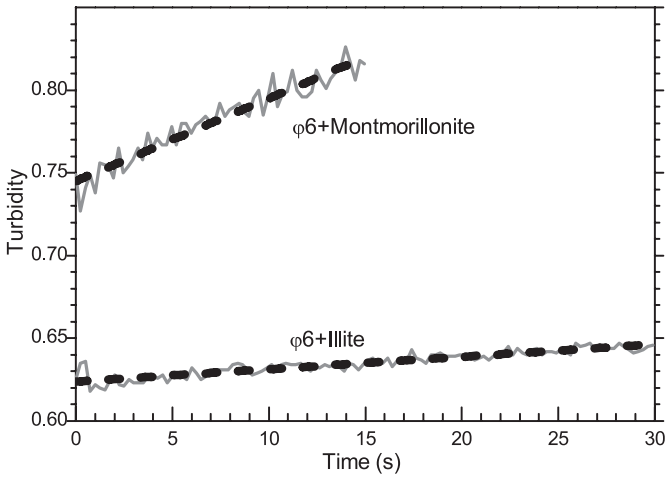

Fig. 3. Time evolution of turbidity (λ = 750 nm) at early time with linear fits (gray diamonds) for φ6-Montmorillonite and φ6-Illite heteroaggregates.

respectively). P1 is the largest molecular weight protein in φ6 and has a relatively high copy number (120 per virion). Thus, P1 is the highest density SDS-PAGE band of all the φ6 proteins.

Viable virus concentrations after aggregation were calculated using the plaque assay technique. The pelleted aggregates were vortexed prior to plaquing to disaggregate the mixture and separate the viruses from the sediments. The supernatants and final, disaggregated, clay suspensions were spot checked on plates with growing *P. phaseolicola* to determine number of virions in the system.

3.5. TEM

Heteroaggregates from the isolated pellets (Section 3.3.3) were prepared for TEM using standard techniques. Samples were negatively stained with uranyl acetate. A minimal amount of stain was employed to reduce the effect of the stain on abundant viral proteins, which would impede identification of viral particles. Micrographs of the heteroaggregates were acquired with a Zeiss 902 TEM operating at 80 keV with a 2048 × 2048 pixel detector. Magnification was 85,000× corresponding to 0.512 nm/pixel. φ6 particles are identifiable in the micrographs from size and morphology. Micrograph insets presented in the Results Section were re-sampled 4:1 using CorelDraw (Version ×8, Corel Corp, Ottawa, Can) to reduce pixelation in the enlarged insets. The contrast of the insets were enhanced using CorelDraw's auto-adjust function.

4. Results and discussion

4.1. Isolated φ6 and sediment turbidity

Prior work (Block et al., 2014) has demonstrated that φ6 does not aggregate in buffer A at neutral pH, therefore $K_{vv} = 0$ (Eq. (6)). It was next confirmed by turbidity measurements that, individually, the four suspended sediments do not aggregate in the dilute buffer. The time evolution of the sediment turbidities at 750 nm, measured over a 900 s time period, are plotted in Figs. 1(A–D). The turbidities remained constant for these measurements, confirming that the cation concentration in the buffer is sufficiently dilute so as to not cause the sediments to aggregate. Thus, K_{ss} in Eq. (6) can be taken to be ≈0 and Eq. (6) simplifies to:

$$\frac{dN_{sv}}{dt} = K_{sv} N_s N_v \tag{9}$$

i.e. primarily hetero-doublets are being formed at early time rather than virus-virus or sediment-sediment doublets. In this case, from Eq. (7), $\frac{d\tau}{dt} \propto K \frac{dN_{sv}}{dt}$, i.e. the rate of hetero-doublet formation.

4.2. Heteroaggregate turbidity

The turbidity of the heteroaggregates at 750 nm is plotted in Fig. 2 (A–D). The φ6-goethite and φ6-kaolinite heteroaggregates demonstrated a linearly increasing turbidity over the entire 900 s time frame of the experiments, indicating that aggregation remained in the linear range, i.e. early stage, and consisted primarily of doublet formation. The turbidity slopes for φ6-goethite and φ6-kaolinite were $2.98 \times 10^{-5} \pm 1.2 \times 10^{-7}\ s^{-1}$ and $2.84 \times 10^{-5} \pm 2.2 \times 10^{-7}\ s^{-1}$, respectively. The respective linear fits to the turbidity are shown in Fig. 2A and C as dotted lines. The least squares linear fit was performed using OriginPro software (OriginLab, Northampton MA, USA). In both the φ6-illite and φ6-montmorillonite heteroaggregates the duration of the linearly increasing turbidity was significantly shorter (30 s for φ6-illite and 15 s for φ6-montmorillonite). The early stage turbidity changes for illite and montmorillonite, along with linear fits, are plotted in Fig. 3. The corresponding slopes during the linear region (primarily doublet formation) are $4.94 \times 10^{-3} \pm 1.9 \times 10^{-4}\ s^{-1}$ for φ6-montmorillonite and $7.50 \times 10^{-4} \pm 2.9 \times 10^{-5}\ s^{-1}$ for the φ6-illite aggregates.

Exact calculations of the heteroaggregation rates from turbidity require knowledge of the scattering cross-sections of both singlets and the doublet (Liu et al., 2007; Yu and Borkovec, 2002). The precise shape of the virus-clay platelet doublet is not well known though there is evidence that virus – clay platelet doublets occur as both

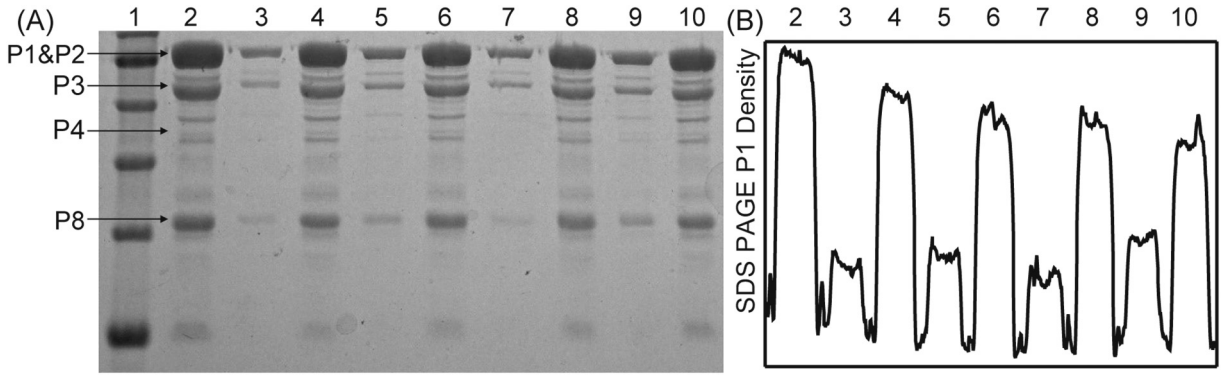

Fig. 4. A) SDS-PAGE of ϕ6 in pellets and supernatants. Lanes are: 1) Marker; 2) Purified ϕ6; 3) ϕ6 — montmorillonite aggregate supernatant; 4) ϕ6 — montmorillonite aggregate pellet; 5) ϕ6 — Kaolinite aggregate supernatant; 6) ϕ6 — Kaolinite aggregate pellet; 7) ϕ6 — Illite aggregate supernatant; 8) ϕ6 — Illite aggregate pellet; 9) ϕ6 — Goethite aggregate supernatant; 10) ϕ6 — Goethite aggregate pellet. B) Density trace of SDS-PAGE for protein band P1, corresponding SDS-PAGE lanes are shown on top of plot. Relative density of pellet and supernatant P1 bands show that the majority of virions are in aggregates.

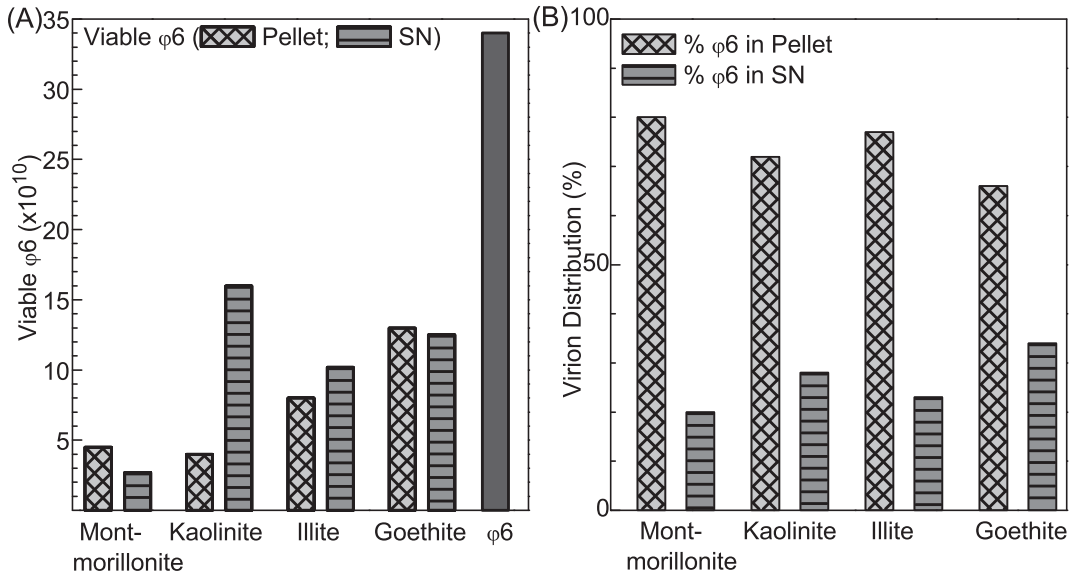

Fig. 5. A) Viable φ6 populations in pellet and supernatant: B) Percentage distribution of virions between pellets and supernatants.

edge-attached and face-attached (Block et al., 2014). Although imprecise knowledge of doublet shape complicates calculations of heteroaggregation rates, analysis of the turbidity slope coupled with particle concentrations allows one to determine relative aggregation rates between φ6 and the four sediment types, elucidating the nature of the interaction.

From the aggregation rates, it is observed that doublet formation occurs at a much slower rate for goethite and kaolinite compared to montmorillonite and illite. That the two positively charged sediments (goethite and kaolinite) aggregate more slowly with the negatively charge virions than the two negatively charged sediments (montmorillonite and illite), it is likely that the interaction between φ6 and the sediments is not electrostatic in nature but hydrophobic, similar to that observed for MS2 and φX174 (Chrysikopoulos and Syngouna, 2012).

4.3. SDS-PAGE and virus viability

The SDS-PAGE of the pellets and supernatants for the four heteroaggregates are plotted in Fig. 4A along with the non-aggregated φ6 control. Comparisons of the density profiles of the P1 and P3 protein bands (Fig. 4B) reveal that for all four heteroaggregates, most of the virions aggregated with the sediments (montmorillonite 80%; kaolinite 73%; illite 76%; goethite 68%) and the remaining non-aggregated virions in the supernatant. It is expected that formation of larger aggregates resulting from either higher cation concentrations or greater sediment concentrations would result in a greater fraction of the virions aggregating. It should be noted that the SDS-PAGE results do not provide information as to virus viability, since the proteins in partially disassembled virions will likely remain intact and thus appear in their respective SDS-PAGE bands.

φ6 viability in the supernatants and pellets as determined by plaquing is presented in Fig. 5a. The distribution of virions (viable and non-viable) is shown in Fig. 5b. The viable virus population in the control was 3.5×10^{11}, in good agreement with our estimates from turbidity (which includes non-infectious virions). φ6 in the montmorillonite aggregates displayed a significant decrease in infectivity for both virions in the aggregates (14% viable) and planktonic cells (35% viable), which is consistent with results from our previous work (Block et al., 2014). In the φ6-kaolinite and φ6-illite aggregates, the virions in the pellets, i.e. aggregated virions, show an appreciable loss in infectivity (14% and 27% of original virus populations remained viable for kaolinite and illite, respectively), while virions that did not aggregate remained close to 100% viable. For the φ6-goethite heteroaggregates, 49% of the virions in the pellets remained viable, while supernatant virion viability was near 100%. The higher viability values for in the φ6-goethite pellet is likely due to fewer virions aggregating as a result of the lower goethite concentration required to achieve approximately equal turbidity as in the experiments with clay minerals to account for goethite's greater refractive index.

4.4. TEM analysis

Analysis of TEM micrographs confirmed the presence of φ6 in each of the four heteroaggregate suspensions. The viruses were observed to be attached to both platelet faces and edges of the three clay minerals. Distortion of the virus morphology was evident in the micrographs (Figs. 6A–D). In the φ6 – goethite heteroaggregates, the virions appear hexagonal with a 55 nm diameter (Fig. 6A). This morphology is consistent with that in micrographs of the icosahedral nucleocapsid (Alimova et al., 2015), indicating that the viral envelope has been disassembled during aggregation with goethite.

Analysis of TEM micrographs of φ6 heteroaggregated with the three clay minerals (Figs. 6B. φ6 – illite; 6C. φ6 – kaolinite; 6D. φ6 – montmorillonite) reveal substantial distortion in the φ6 morphology. The viral particle diameters are similar to the 55 nm diameter of the nucleocapsid rather than the 80 nm diameter of the intact virions and the virions appear to be distinctly non-circular. The morphologic changes indicate that the sediments partially disassembled the viral envelope – a process likely responsible for the reduced rate of virus infectivity.

5. Conclusions

Turbidity measurements on dilute combinations of bacteriophage φ6 and four sediment types were collected to determine the relative rates of heteroaggregation. Negatively charged sediments aggregated with φ6 at a faster rate than positively charged sediments, indicating that the interaction is not electrostatic, but hydrophobic in nature. Because K, the rate constant, is independent of concentration, the relative rates for aggregation at low turbidity are a good predictor of rates at higher concentrations.

For all experiments, most of the virions aggregated with sediments regardless of mineral type. At higher sediment

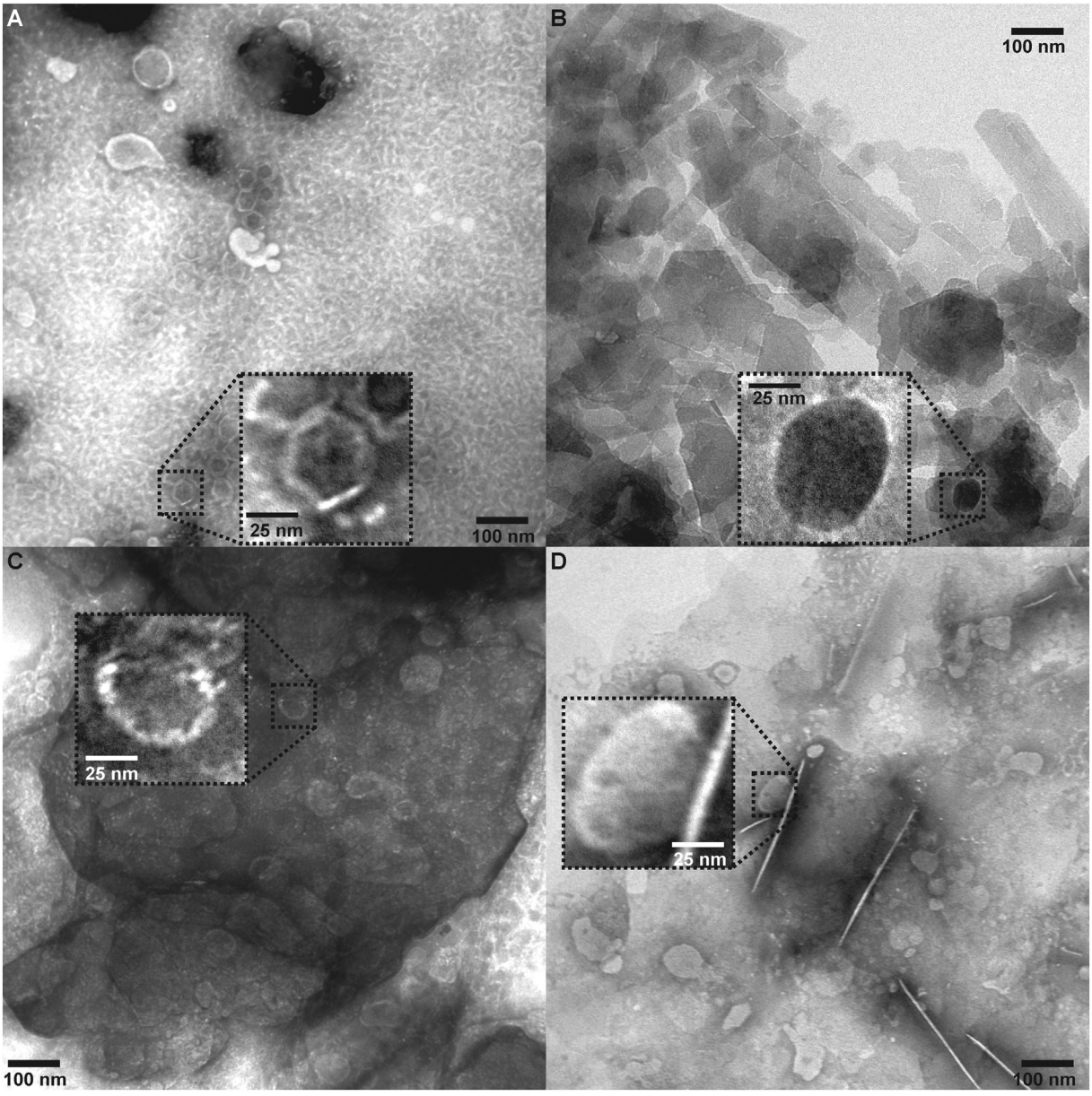

Fig. 6. TEM Micrograph of heteroaggregates of φ6 and A) Goethite, C) Kaolinite and D) Montmorillonite. Insets show enlarged view (contrast (enhanced) of individual virions in the aggregates. φ6 viruses in the aggregates demonstrate significant distortion as compared to isolated φ6.

concentrations, we expect an even larger viral fraction to aggregate, resulting in higher deposition rates. Nevertheless, at the low concentrations of our experiments, heteroaggregated viruses experienced a loss of infectivity. Despite the fragility of the viral envelope, a large number of virions remained viable, indicating that small-sized heteroaggregates may pose an infection risk. While non-aggregated virions in the φ6 – goethite, φ6 –kaolinite and φ6 – illite suspensions remained near 100% viable, in the φ6 – montmorillonite suspensions, a substantial fraction (35%) of the non-aggregated φ6 also lost viability. TEM analysis revealed that the observed reduction in infectivity is likely due to partial disassembly of the viral envelope after aggregation. In conclusion, it is expected that viral disassembly and loss of infectivity is likely to be exacerbated with increased contact between virions and sediments which occurs within larger aggregates.

The formation of sediment-virus heteroaggregates and subsequent virus inactivation has potential implications for remediation, spread of disease, and management of wastewater particularly during reintroduction via porous media into groundwater systems. Our results suggest that soils containing clay minerals, and in particular, montmorillonite, may potentially serve to inactivate viruses possessing a rigid lipid envelopes during colloidal transport. However, our results also show that even in the case of viruses that are not inactivated by association with a solid phase, colloidal sediments could facilitate the transport of viruses into aquifers as small heteroaggregates. Furthermore, because multiple virions aggregate with colloidal sediment even in dilute concentrations, forming heteroaggregates in the colloidal size range, this interaction must be considered in conjunction with specific infectivity (Ghanem et al., 2018) when phages are used in tracer experiments.

Acknowledgements

Partial support for this project was provided by PSC-CUNY Award TRADA-46-247, jointly funded by the Professional Staff Congress and the City University of New York.

References

Alimova, A., Katz, A., Sriramoju, V., Budansky, Y., Bykov, A.A., Zeylikovich, R., R, A.R., 2006. In: Katz, A., Alfano, R.R. (Eds.), Hybrid Native Phosphorescence and Fluorescence Spectroscopy for Cancer Detection. SPIE Proc., San Jose, CA, pp. 22–25.

Alimova, A., Katz, A., Steiner, N., Rudolph, E., Hui, W., Steiner, J.C., Gottlieb, P., 2009. Bacteria-clay interaction: structural changes in smectite induced during biofilm formation. Clay Clay Miner. 57 (2), 205–212.

Alimova, A., Wei, H., Katz, A., Spatz, L., Gottlieb, P., 2015. The ϕ6 cystovirus protein P7 becomes accessible to antibodies in the transcribing nucleocapsid: a probe for viral structural elements. PLoS One 10 (3), e0122160. https://doi.org/10.1371/journal.pone.0122160.

Batik, O., Craun, G.F., Tuthill, R.W., Kraemer, D.F., 1980. An epidemiologic study of the relationship between hepatitis A and water supply characteristics and treatment. Am. J. Public Health 70 (2):167–168. https://doi.org/10.2105/ajph.70.2.167.

Block, K.A., Trusiak, A., Katz, A., Gottlieb, P., Alimova, A., Wei, H., Morales, J., Rice, W.J., Steiner, J.C., 2014. Disassembly of the cystovirus ϕ6 envelope by montmorillonite clay. MicrobiologyOpen 3 (1):42–51. https://doi.org/10.1002/mbo3.148.

Block, K.A., Katz, A., Alimova, A., Trusiak, A., Morales, J., Wei, H., Bucher, D., Gottlieb, P., 2016. Montmorillonite-mediated aggregation induces deformation of influenza virus particles. Appl. Clay Sci. 124–125:211–218. https://doi.org/10.1016/j.clay.2016.02.010.

Breitbart, M., Rohwer, F., 2005. Here a virus, there a virus, everywhere the same virus? Trends Microbiol. 13 (6):278–284. https://doi.org/10.1016/j.tim.2005.04.003.

Chattopadhyay, S., Puls, R.W., 1999. Adsorption of bacteriophages on clay minerals. Environ. Sci. Technol. 33 (20):3609–3614. https://doi.org/10.1021/es9811492.

Chattopadhyay, S., Puls, R.W., 2000. Forces dictating colloidal interactions between viruses and soil. Chemosphere 41 (8), 1279–1286.

Chrysikopoulos, C.V., Syngouna, V.I., 2012. Attachment of bacteriophages MS2 and ϕX174 onto kaolinite and montmorillonite: extended-DLVO interactions. Colloids Surf. B: Biointerfaces 92:74–83. https://doi.org/10.1016/j.colsurfb.2011.11.028.

Chu, Y., Jin, Y., Yates, M.V., 2000. Virus transport through saturated sand columns as affected by different buffer solutions. J. Environ. Qual. 29 (4), 1103–1110.

Chýlek, P., Li, J., 1995. Light scattering by small particles in an intermediate region. Opt. Commun. 117 (5), 389–394.

Deer, W.A., Howie, R.A., Zussman, J., 1992. An Introduction to the Rrock-Forming Minerals. Longman Scientific & Technical, Hong Kong.

Dennehy, J.J., 2017. Evolutionary ecology of virus emergence. Ann. N. Y. Acad. Sci. 1389 (1):124–146. https://doi.org/10.1111/nyas.13304.

Derjaguin, B., Landau, L., 1941. Theory of the stability of strongly charged lyophobic sols and of the adhesion of strongly charged particles in solution of electrolytes. Acta Physicochim. 14, 633–662.

Díaz-Muñoz, S.L., Koskella, B., 2014. Bacteria–phage interactions in natural environments. Adv. Appl. Microbiol. 89:135–183. https://doi.org/10.1016/B978-0-12-800259-9.00004-4.

Elimelech, M., Gregory, J., Jia, X., Williams, R., 1995. Particle Deposition and Aggregation: Measurement, Modelling and Simulation. Butterworth-Heinemann.

Flood, J.A., Ashbolt, N.J., 2000. Virus-sized particles can be entrapped and concentrated one hundred fold within wetland biofilms. Adv. Environ. Res. 3 (4), 403–411.

Fuhrman, J.A., 1999. Marine viruses and their biogeochemical and ecological effects. Nature 399 (6736), 541.

Gaboriaud, F., Ehrhardt, J.-J., 2003. Effects of different crystal faces on the surface charge of colloidal goethite (α-FeOOH) particles: an experimental and modeling study. Geochim. Cosmochim. Acta 67 (5):967–983. https://doi.org/10.1016/S0016-7037(02)00988-2.

García-García, S., Jonsson, M., Wold, S., 2006. Temperature effect on the stability of bentonite colloids in water. J. Colloid Interface Sci. 298 (2):694–705. https://doi.org/10.1016/j.jcis.2006.01.018.

García-García, S., Wold, S., Jonsson, M., 2007. Kinetic determination of critical coagulation concentrations for sodium- and calcium-montmorillonite colloids in NaCl and $CaCl_2$ aqueous solutions. J. Colloid Interface Sci. 315 (2):512–519. https://doi.org/10.1016/j.jcis.2007.07.002.

Ghanem, N., Trost, M., Sánchez Fontanet, L., Harms, H., Chatzinotas, A., Wick, L.Y., 2018. Changes of the specific infectivity of tracer phages during transport in porous media. Environ. Sci. Technol. 52 (6):3486–3492. https://doi.org/10.1021/acs.est.7b06271.

González Sánchez, F., Van Loon, L.R., Gimmi, T., Jakob, A., Glaus, M.A., Diamond, L.W., 2008. Self-diffusion of water and its dependence on temperature and ionic strength in highly compacted montmorillonite, illite and kaolinite. Appl. Geochem. 23 (12):3840–3851. https://doi.org/10.1016/j.apgeochem.2008.08.008.

Gundy, P.M., Gerba, C.P., Pepper, I.L., 2008. Survival of coronaviruses in water and wastewater. Food Environ. Virol. 1 (1):10. https://doi.org/10.1007/s12560-008-9001-6.

Gupta, V., Hampton, M.A., Stokes, J.R., Nguyen, A.V., Miller, J.D., 2011. Particle interactions in kaolinite suspensions and corresponding aggregate structures. J. Colloid Interface Sci. 359 (1):95–103. https://doi.org/10.1016/j.jcis.2011.03.043.

Jin, Y., Flury, M., 2002. In: Sparks, D.L. (Ed.), Advances in Agronomy. Academic Press, San Diego, CA, pp. 39–102.

Katz, G., Wei, H., Alimova, A., Katz, A., Morgan, D.G., Gottlieb, P., 2012. Protein P7: A Molecular Bracket in the Cystovirus ϕ6 Procapsid (New York, NY).

Katz, A., Block, K.A., Trusiak, A., Gottlieb, P., Alimova, A., Wei, H., Morales, J., Rice, W.J.R., Steiner, J.C., 2013. Disassembly of phage ϕ6 by montmorillonite clay. AGU Chapman Conference Tucson, AZ, p. T47.

Keswick, B.H., Wang, D.S., Gerba, C.P., 1982. The use of microorganisms as ground-water tracers: a review. Groundwater 20 (2):142–149. https://doi.org/10.1111/j.1745-6584.1982.tb02741.x.

Kimura, M., Jia, Z.-J., Nakayama, N., Asakawa, S., 2008. Ecology of viruses in soils: past, present and future perspectives. Soil Sci. Plant Nutr. 54 (1):1–32. https://doi.org/10.1111/j.1747-0765.2007.00197.x.

Kobayashi, M., Ishibashi, D., 2011. Absolute rate of turbulent coagulation from turbidity measurement. Colloid Polym. Sci. 289 (7):831–836. https://doi.org/10.1007/s00396-011-2388-x.

Koskella, B., Brockhurst, M.A., 2014. Bacteria–phage coevolution as a driver of ecological and evolutionary processes in microbial communities. FEMS Microbiol. Rev. 38 (5), 916–931.

Liu, J., Xu, S., Sun, Z., 2007. Toward an understanding of the turbidity measurement of heterocoagulation rate constants of dispersions containing particles of different sizes. Langmuir 23 (23):11451–11457. https://doi.org/10.1021/la701426u.

McGechan, M.B., Lewis, D.R., 2002. SW—soil and water transport of particulate and colloid-sorbed contaminants through soil, part 1: general principles. Biosyst. Eng. 83 (3):255–273. https://doi.org/10.1006/bioe.2002.0125.

Mindich, L., 2004. Packaging, replication and recombination of the segmented genome of bacteriophage Φ6 and its relatives. Virus Res. 101 (1):83–92. https://doi.org/10.1016/j.virusres.2003.12.008.

O'Brien, E., Munir, M., Marsh, T., Heran, M., Lesage, G., Tarabara, V.V., Xagoraraki, I., 2017. Diversity of DNA viruses in effluents of membrane bioreactors in Traverse City, MI (USA) and La Grande Motte (France). Water Res. 111:338–345. https://doi.org/10.1016/j.watres.2017.01.014.

Puertas, A.M., Nieves, F.J.d.l., 1997. A new method for calculating kinetic constants within the Rayleigh - Gans - Debye approximation from turbidity measurements. J. Phys. Condens. Matter 9 (16), 3313.

Redman, J., Grant, S., Olson, T., Hardy, M., Estes, M., 1997. Filtration of recombinant Norwalk virus particles and bacteriophage MS2 in quartz sand: importance of electrostatic interactions. Environ. Sci. Technol. 31 (12), 3378–3383.

Rosenberg, M.L., Koplan, J.P., Pollard, R.A., 1980. The risk of acquiring hepatitis from sewage-contaminated water. Am. J. Epidemiol. 112 (1), 17–22.

Schroth, B.K., Sposito, G., 1997. Surface charge properties of kaolinite. Clay Clay Miner. 45 (1), 85–91.

Shannon, R.D., Shannon, R.C., Medenbach, O., Fischer, R.X., 2002. Refractive index and dispersion of fluorides and oxides. J. Phys. Chem. Ref. Data 31 (4):931–970. https://doi.org/10.1063/1.1497384.

Sharp, D.G., Floyd, R., Johnson, J.D., 1975. Nature of the surviving plaque-forming unit of reovirus in water containing bromine. Appl. Microbiol. 29 (1), 94–101.

Stallknecht, D.E., Kearney, M.T., Shane, S.M., Zwank, P.J., 1990a. Effects of pH, temperature, and salinity on persistence of avian influenza viruses in water. Avian Dis. 34 (2), 412–418.

Stallknecht, D.E., Shane, S.M., Kearney, M.T., Zwank, P.J., 1990b. Persistence of avian influenza viruses in water. Avian Dis. 34 (2), 406–411.

Studier, F.W., 1973. Analysis of bacteriophage T7 early RNAs and proteins on slab gels. J. Mol. Biol. 79 (2), 237–248.

Syngouna, V.I., Chrysikopoulos, C.V., 2015. Experimental investigation of virus and clay particles cotransport in partially saturated columns packed with glass beads. J. Colloid Interface Sci. 440:140–150. https://doi.org/10.1016/j.jcis.2014.10.066.

Van Olphen, H., 1962. Unit layer interaction in hydrous montmorillonite systems. J. Colloid Sci. 17 (7):660–667. https://doi.org/10.1016/0095-8522(62)90030-2.

van Oss, C.J., 1993. Acid—base interfacial interactions in aqueous media. Colloids Surf. A Physicochem. Eng. Asp. 78 (0):1–49. https://doi.org/10.1016/0927-7757(93)80308-2.

van Oss, C.J., Giese, R.F., Costanzo, P.M., 1990. DLVO and non-DLVO interactions in hectorite. Clay Clay Miner. 38 (2), 151–159.

Verwey, E.J.W., Overbeek, J.T.G., 1948. Theory of the Stability of Lyophobic Colloids. Elsevier Publishing, New York.

Vilker, V.L., Lyklema, J., Norde, W., Verduin, B.J.M., 1994. Interaction between a plant virus and colloidal hematite. Water Res. 28 (12):2425–2432. https://doi.org/10.1016/0043-1354(94)90060-4.

Weidler, P.G., Friedrich, F., 2007. Determination of the refractive index of particles in the clay and sub-micrometer size range. Am. Mineral. 92 (7):1130–1132. https://doi.org/10.2138/am.2007.2313.

Weinbauer, M.G., Rassoulzadegan, F., 2004. Are viruses driving microbial diversification and diversity? Environ. Microbiol. 6 (1), 1–11.

Wind, L., Szymanski, W.W., 2002. Quantification of scattering corrections to the Beer-Lambert law for transmittance measurements in turbid media. Meas. Sci. Technol. 13 (3), 270.

Xu, M., 2003. Light extinction and absorption by arbitrarily oriented finite circular cylinders by use of geometrical path statistics of rays. Appl. Opt. 42 (33):6710–6723. https://doi.org/10.1364/AO.42.006710.

Xu, S., Sun, Z., 2010. Evaluation of the uncertainties caused by the forward scattering in turbidity measurement of the coagulation rate. Langmuir 26 (10):6908–6918. https://doi.org/10.1021/la904155y.

Xu, M., Lax, M., Alfano, R.R., 2003. Anomalous diffraction of light with geometrical path statistics of rays and a Gaussian ray approximation. Opt. Lett. 28 (3):179–181. https://doi.org/10.1364/OL.28.000179.

Yu, W.L., Borkovec, M., 2002. Distinguishing heteroaggregation from homoaggregation in mixed binary particle suspensions by multiangle static and dynamic light scattering. J. Phys. Chem. B 106 (51):13106–13110. https://doi.org/10.1021/jp021792h.

Zeltner, W.A., Anderson, M.A., 1988. Surface charge development at the goethite/aqueous solution interface: effects of CO_2 adsorption. Langmuir 4 (2):469–474. https://doi.org/10.1021/la00080a039.